PENA TEKNIK
JURNAL ILMIAH ILMU - ILMU TEKNIK

*Vol. 10, No.02, September (2025)*
*p-ISSN 2502-8952*
*e-ISSN 2623-2197*
*https://ojs.unanda.ac.id/index.php/jiit/index*

# Analysis of Variation in the Number of Layers in the Hardfacing Process of ASTM A216 WCB Material on Hardness, Wear, and Microstructure

Alvalo Toto Wibowo [1,*], Mochammad Karim Al Amin [1], Mohammad Thoriq Wahyudi [1], Hendri Budi Kurniyanto [1], Moh. Syaiful Amri [1], Moch. Aria Firmansyah [1], Rikky Leonard [2], Alvido Toto Wijaya [3]

[1] *D4 Teknik Pengelasan, Politeknik Perkapalan Negeri Surabaya, Jalan Teknik Kimia Kampus ITS, Surabaya, 6011, Indonesia*
[2] *D4 Teknologi Rekayasa Konstruksi Kapal, Politeknik Perkapalan Negeri Surabaya, Jalan Teknik Kimia Kampus ITS, Surabaya, 6011, Indonesia*
[3] *S1 Teknik Mesin, Universitas Trunojoyo Madura, Jalan Raya Telang, Bangkalan, 69161, Indonesia*
** Corresponding Author E-mail: : alvalototo@ppns.ac.id*

**Keywords:**
Buffer layer ; Hardfacing ; Hardness ; Wear Resistance; Microstructure

**Abstract**

ASTM A216 WCB material is a cast carbon steel commonly used in valve components operating at high temperatures, where one of the main problems is surface wear. This study aims to analyze the effect of variations in the number of Stellite 12 hardfacing layers and the type of buffer layer (ER308 and ER309) on the hardness, wear resistance, and microstructure of ASTM A216 WCB material. Four variations of specimens were tested using the Gas Tungsten Arc Welding (GTAW) welding process. The hardness test results showed that increasing the number of layers consistently increased the material hardness due to reduced dilution and microstructural refinement. The highest hardness value of 477.89 HV was recorded in the specimen with the ER309 buffer layer and four layers of hardfacing. In contrast, the lowest wear rate, which indicates the highest wear resistance, was 0.00318 $mm^3/Nm$ and was observed in the specimen with the ER308 buffer layer and two layers of hardfacing, which had a lower surface hardness (396.13 HV). These results indicate a non-linear relationship between maximum hardness and optimal wear performance. Microstructural observations indicate that the base metal has a ferrite and pearlite structure. In the buffer layer, austenite and vermicular ferrite structures are formed. Meanwhile, in the hardfacing layer, α-dendritic phases and complex carbide precipitation were found, which were presumptively identified as M23C6. This study concludes that optimizing hardfacing performance on WCB steel requires a balance between the hardness achieved through the number of layers and the microstructural toughness influenced by the interaction with the buffer layer.

## 1. INTRODUCTION

The rapid development of the industrial sector has led to an increase in the use of pipes as a means of transporting water, oil, gas, and various other types of fluids. In a piping system, there is an element known as a valve. A valve is a mechanical component specifically designed to control, regulate, and guide the speed of fluid flow by opening, closing, or partially opening the flow pressure rate (Maulana et al., 2020). In addition to opening or closing the flow, the valve also functions to regulate flow speed, direct flow, prevent backflow, control pressure, or reduce pressure (Yusim et al., 2020). Valves have an important part, one of which is the disc component. The valve disc is a component that functions to control the flow of fluid through the valve. The disc is the part that experiences direct friction with the fluid, so increasing its hardness is very important, as it can improve resistance to damage caused by friction. The carbon steel material that is usually used is the ASTM A216 WCB type. This material is widely used in the valve body manufacturing process because of its balance of mechanical properties, toughness, and ease of fabrication process up to temperatures of 425°C (JC Casting, 2025).

**doi** https://doi.org/10.51557/yknegr07
**article history**: Received June 19, 2025; Received in revised from August 19, 2025; Accepted September 22, 2025; Available online September 30, 2025.

This is an open access article under the **CC-BY-SA** license

ASTM A216 WCB material is resistant to wear, but when used in the field, wear will decrease, causing a short service life and high maintenance costs. Therefore, it is necessary to coat the surface of the material to improve the performance and durability of the material using hardfacing. Hardfacing is used on parts that experience extreme wear, impact, and corrosion (Tandon et al., 2023). This method can also increase surface resistance in low-carbon steel (Chotěborský et al., 2008) in (Susetyo et al., 2021). Hardfacing overlay is a process of hardening a metal surface by adding a filler metal that has high wear resistance and hardness to the base metal surface (Jong et al., 2021). Hardfacing can be applied to new components during their manufacture or to restore worn surfaces (Garbade et al., 2021). Among various hardfacing alloys, cobalt-based alloys such as Stellite are known to have superior wear resistance, corrosion resistance, and high-temperature hardness retention, mainly due to their microstructure consisting of a cobalt-chromium (Co-Cr) matrix strengthened by hard carbide precipitation (Gonçalves Júnior et al., 2024).

Welding is an inseparable part of industrial development because of its role in the engineering process and product repair of metal materials (Herizal et al., 2020). Gas Tungsten Arc Welding (GTAW) is carried out by heating the metal until it melts using an electric arc formed from tungsten and a metal electrode. The electrode functions as a support for the creation of an electric arc; this classifies GTAW electrodes as non-consumable electrodes. (Abdullah et al., 2021). Gas Tungsten Arc Welding (GTAW) is a welding process that has good visual quality and is a precision welding process (Badheka et al., 2016). Welding parameters such as welding current, arc voltage, welding speed, torch angle, welding wire length, nozzle distance, welding position and direction, and welding flow rate (Karadeniz et al., 2007) in (Azwinur et al., 2020). Heat input in welding greatly affects the phase structure, cooling rate, and distortion (Fauzi et al., 2024). Optimal buffer layer selection is an important technique to reduce the propagation of defects from the substrate to the coating and prevent the occurrence of defects due to stress after the welding process (Rana et al., 2023).

According to the Schaeffler diagram, which predicts the microstructural phases in stainless steel welds based on chromium and nickel equivalents, ER309 has a higher alloy content than ER308 (Australian Stainless Steel Development Association, 2012). Darmo and Prihadianto performed hardfacing with AWS A5.13 electrodes (JIS Z 3251) on steel with varying manganese content of 10.4, 11.6, 12.7, 13.6, and 14.6 wt.%, resulting in hardness between 230 and 250 HV (Darmo et al., 2023). Susetyo et al. performed a hardfacing process using three layers of AWS A5.13 EFe2 electrodes interspersed with E7018 electrodes as buffer layers and current variations of 90, 110, and 130 A, resulting in the highest hardness in samples welded with a current of 130 A (Susetyo et al., 2021). The high alloy content of ER309 provides resistance to Fe dilution from carbon steel, thereby preventing the formation of a brittle martensite phase and producing a more ductile joint. In contrast, the performance of ER308, which has a lower alloy content, is more sensitive to process parameters and the level of dilution. In addition to buffer layer selection, the number of hardfacing layers is also a critical parameter for controlling dilution. Multi-layer deposition ensures the surface layer has the purest chemical composition for optimal wear resistance. Furthermore, the repeated thermal cycles of this process serve as an in-situ heat treatment that refines the dendritic structure, distributes carbides homogeneously, and ultimately increases hardness (Luijan et al., 2023).

Although the principle of hardfacing is well understood, systematic comparative studies on the interactive effects between the type of buffer layer (ER308 vs. ER309) and the number of Stellite 12 hardfacing layers on ASTM A216 WCB substrates are still very limited, as existing studies tend to focus on a single variable. Therefore, the research gap in this study is the lack of understanding of how the specific combination of these two factors simultaneously affects the evolution of the resulting hardness, wear, and microstructure values. The novelty of this study lies in the systematic investigation of these interactions, with the aim of identifying the relationships between process parameters, structure, and properties, and revealing the potential for an optimal balance between maximum hardness and highest wear resistance for industrial applications.

## 2. METHOD

The basic material used in this study is ASTM A216 WCB cast carbon steel with dimensions of 150 mm × 150 mm × 10 mm. The filler metals used are ER308 and ER309 as buffer layer s and Stellite 12 as hardfacing layer material. The chemical composition of ASTM A216 WCB material is presented in Table 1. This study uses a factorial design that produces four variations of specimens by varying the type of buffer layer (ER308 and ER309) and the number of hardfacing layers (two and four layers). The welding process used is Gas Tungsten Arc Welding (GTAW) with a downhand welding position (1G). The welding parameters used for each specimen are detailed in Table 2.

Table 1. Chemical Composition of ASTM A216 WCB

| ***Grade*** | **C** | **M N** | **Si** | **S** | **P** | **CR** | **This** | **Mo** | **Cu** | **V** |
|---|---|---|---|---|---|---|---|---|---|---|
| ASTM A216 WCB | 0.3 | 1 | 0.6 | 0.035 | 0.035 | 0.5 | 0.5 | 0.2 | 0.3 | 0.003 |

Table 2. Welding Parameters

| ***Marking*** | **Electrode** | ***Ampere*** **(A)** | ***Voltage*** **(V)** | ***Layer of Weld*** | ***Travel Speed*** **(mm/min)** | ***Heat Input*** **(KJ/mm)** |
|---|---|---|---|---|---|---|
| Specimen 1 | ER308 | 135 | 13 | *Layer* 1 | 61.73 | 1.81764 |
| | | | | *Layer* 2 | 64.38 | 1.95696 |
| | Stellite 12 | 145 | 14 | *Layer* 3 | 64.38 | 1.95692 |
| | | | | *Layer* 4 | 63.56 | 1.91632 |
| Specimen 2 | ER308 | 135 | 12 | *Layer* 1 | 59.29 | 1.98936 |
| | | | | *Layer* 2 | 59.06 | 1,79388 |
| | Stellite 12 | 145 | 13 | *Layer* 3 | 64.38 | 1.78698 |
| | | | 14 | *Layer* 4 | 64.66 | 1.95692 |
| | | | | *Layer* 5 | 63.03 | 1.98940 |
| | | | | *Layer* 6 | 62.73 | 1.96504 |
| Specimen 3 | ER309 | 135 | 12 | *Layer* 1 | 60.24 | 1.63944 |
| | | | | *Layer* 2 | 63.03 | 1,62000 |
| | Stellite 12 | 145 | 14 | *Layer* 3 | 63.03 | 2.02188 |
| | | | | *Layer* 4 | 62.76 | 1.96504 |
| Specimen 4 | ER309 | 135 | 12 | *Layer* 1 | 61.98 | 1.69884 |
| | | | | *Layer* 2 | 61.73 | 1,70586 |
| | Stellite 12 | 145 | 13 | *Layer* 3 | 64.10 | 1.94068 |
| | | | 14 | *Layer* 4 | 63.56 | 1.96504 |
| | | | | *Layer* 5 | 63.83 | 2,00564 |
| | | | | *Layer* 6 | 64.38 | 1.94880 |

After the welding process, a series of tests were conducted for characterization. Vickers hardness testing was performed using a load of 10 kgf with a holding time of 12 seconds. Indentations were performed on the base metal, HAZ, both buffer layers, and each hardfacing layer. This study was exploratory in nature to identify metallurgical trends and phenomena. Each condition variation was represented by one specimen (n=1). Therefore, inferential statistical analysis such as two-factor ANOVA cannot be applied to claim statistical significance. Claims in this manuscript are based on the analysis of trends observed from the data and supported by metallurgical principles. Hardness testing was performed with three indentations per location to provide a measure of local variability. Wear performance was evaluated using the pin-on-disc method in accordance with ASTM G99-17, Standard Test Method for Wear Testing with a Pin-on-Disk Apparatus. The pin-shaped test specimens were cut from the layer of hardfacing on top of every variation. Testing is done by pressing the pin on the disc coated with rotating abrasive SiC paper with 60 grit. The test parameters used are a normal load

of 1086 g (10.65 N), a trail radius of 100.58 mm, a spin speed of 1326.2 RPM, and a duration of 1 minute. For microstructure analysis, the specimen was cut transversely, polished, and etched in a chemical way. Two types of reagent etching were used: Nital solution (3% $HNO_3$ in ethanol) for the base metal and HAZ areas, as well as Aqua Regia solution (1 part $HNO_3$ and 3 parts HCl) for the buffer layer and hardfacing layer areas. Observation of the microstructure is done using microscope optics

## 3. RESULT AND DISCUSSION

### 3.1 Hardness Testing

Hardness testing was carried out to determine the hardness value of each specimen from various variations in this study, including the base metal, HAZ, buffer layer, and each layer of the hardfacing layer.

Table 3. Hardness Test Results

| Variation | Location | Hardness Test Value (HV) | | | Average (HV) |
|---|---|---|---|---|---|
| | | To 1 | 2nd | The 3rd | |
| Specimen 1 (Buffer layer ER308, 2 Layer Hardfacing) | Base metal | 157.13 | 163.35 | 155.95 | 158.81 |
| | HAZ | 164.61 | 171.55 | 231.98 | 189.38 |
| | Buffer layer 1 | 261.35 | 274.05 | 265.93 | 267.11 |
| | Buffer layer 2 | 329.24 | 279.5 | 261.91 | 290.22 |
| | Hardfacing Layer 1 | 315.66 | 361.07 | 352.00 | 342.91 |
| | Hardfacing Layer 2 | 379.94 | 412.90 | 395.54 | 396.13 |
| Specimen 2 (Buffer layer ER308, 4 Layer Hardfacing) | Base metal | 160.48 | 157.86 | 160.38 | 159.57 |
| | HAZ | 167.50 | 155.54 | 160.33 | 161.12 |
| | Buffer layer 1 | 307.49 | 319.08 | 317.49 | 314.69 |
| | Buffer layer 2 | 361.71 | 389.23 | 386.39 | 379.11 |
| | Hardfacing Layer 1 | 403.52 | 440.31 | 423.83 | 422.55 |
| | Hardfacing Layer 2 | 411.74 | 444.85 | 470.77 | 442.45 |
| | Hardfacing Layer 3 | 443.33 | 502.14 | 502.41 | 482.63 |
| | Hardfacing Layer 4 | 442.68 | 489.25 | 455.04 | 465.32 |
| Specimen 3 (Buffer layer ER309, 2 Layer Hardfacing) | Base metal | 157.77 | 162.86 | 158.78 | 159.81 |
| | HAZ | 174.24 | 170.87 | 168.25 | 171.12 |
| | Buffer layer 1 | 181.85 | 212.11 | 206.14 | 200.03 |
| | Buffer layer 2 | 373.66 | 206.55 | 210.96 | 263.72 |
| | Hardfacing Layer 1 | 436.47 | 408.46 | 418.02 | 420.98 |

| Variation | Location | Hardness Test Value (HV) | | | Average (HV) |
|---|---|---|---|---|---|
| | | To 1 | 2nd | The 3rd | |
| | Hardfacing Layer 2 | 474.11 | 462.34 | 437.74 | 458.06 |
| Specimen 4 (Buffer layer ER309, 4 Layer Hardfacing) | Base metal | 153.22 | 167.8 | 159.3 | 160.11 |
| | HAZ | 168.86 | 173.65 | 167.60 | 170.04 |
| | Buffer layer 1 | 262.63 | 283.34 | 232.72 | 259.36 |
| | Buffer layer 2 | 267.63 | 408.65 | 248.4 | 308.23 |
| | Hardfacing Layer 1 | 343.71 | 351.24 | 352.77 | 349.24 |
| | Hardfacing Layer 2 | 345.65 | 483.10 | 490.34 | 439.70 |
| | Hardfacing Layer 3 | 459.59 | 486.41 | 465.36 | 464.45 |
| | Hardfacing Layer 4 | 495.67 | 469.35 | 468.64 | 477.89 |

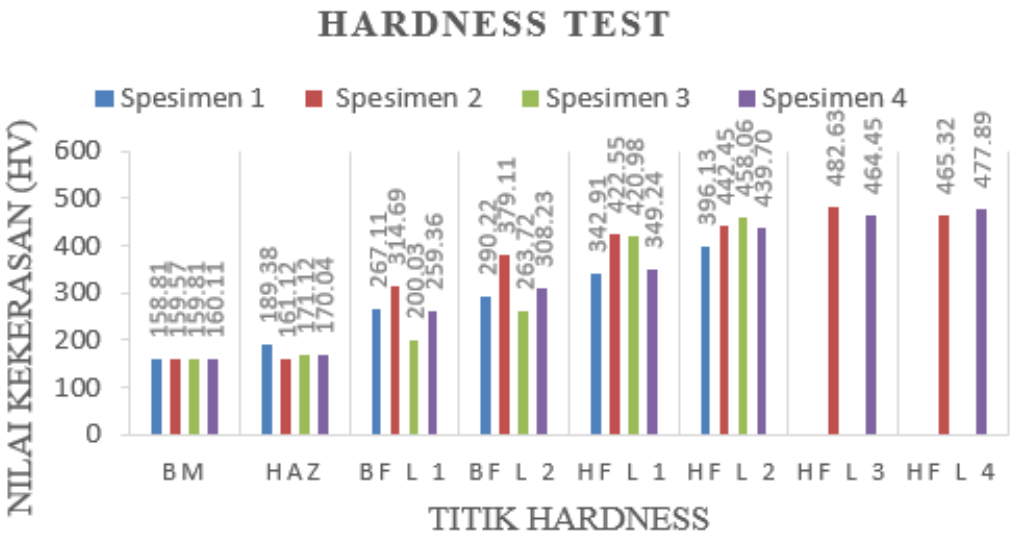



Figure 1: Hardness Test Results Graph

The average hardness of the ASTM A216 WCB base metal was consistent across the four specimens, ranging from 158.81 HV to 160.11 HV, consistent with the characteristics of cast carbon steel in its initial state. In the HAZ, a slight increase in hardness was observed, caused by the thermal cycle of welding that produces grain refinement, thus increasing the resistance to dislocation movement. The buffer layer showed a significant increase in hardness. There was a clear difference in performance between the ER308 (Specimens 1 and 2) and ER309 (Specimens 3 and 4) buffer layers. The specimens using ER308 consistently produced harder buffer layers. This difference is most likely due to the chemical composition. ER309 has higher Cr and Ni contents, which stabilize the softer and more ductile austenite phase and are more resistant to carbon dilution from the base metal. In contrast, ER308 with a lower alloy content may experience greater carbon pickup from the base metal, which may induce precipitation hardening or partial phase transformation. The Stellite 12 hardfacing layer exhibited the highest hardness increase, which is attributed to its microstructure consisting of a cobalt matrix reinforced by the precipitation of very hard complex carbides (Senthilkumar et al., 2023).

Data analysis revealed two main trends. First, increasing the number of layers from two to four consistently increased the hardness of the surface layer. The highest hardness value in the two-layer specimen (Specimen 3) was 458.06 HV, while in the four-layer specimen (Specimen 4) it reached 477.89 HV. Consequently, the top layer has a chemical composition closest to that of pure Stellite 12, allowing for the formation of a higher carbide volume fraction. Second, the hardness gradually increased with each additional layer (HF L1 to HF L4) in Specimens 2 and 4. For example, in Specimen 2, the hardness increased from 422.55 HV (HF L1) to 465.32 HV (HF L4). This phenomenon is due to the repeated thermal cycles of subsequent layer deposition acting as an in-situ heat treatment of the underlying layer, promoting grain refinement and homogenization of the structure. This confirms that to achieve optimal surface properties of Stellite alloys, multi-layer deposition is necessary to overcome the dilution effect. Overall, the measured hardness profiles provide strong evidence that the combination of buffer layer type and number of hardfacing layers interactively determines the hardness distribution across the weld deposit. The highest hardness value achieved by Specimen 4 (ER309, 4 layers) indicates that the use of a metallurgically stable buffer layer combined with a sufficient number of layers is an effective strategy for maximizing surface hardness.

### 3.2 Wear Testing

The wear performance was evaluated based on the specific wear rate (mm³/Nm), where lower values indicate higher wear resistance. The test results showed that all hardfacing configurations drastically improved the wear resistance compared to the ASTM A216 WCB base material. The wear rate of the base material was 0.01338 mm³/Nm, while all coated specimens had wear rates below 0.006 mm³/Nm. The most prominent finding is the existence of a non-linear relationship between surface hardness and wear resistance, which is often referred to as the hardness-wear paradox.

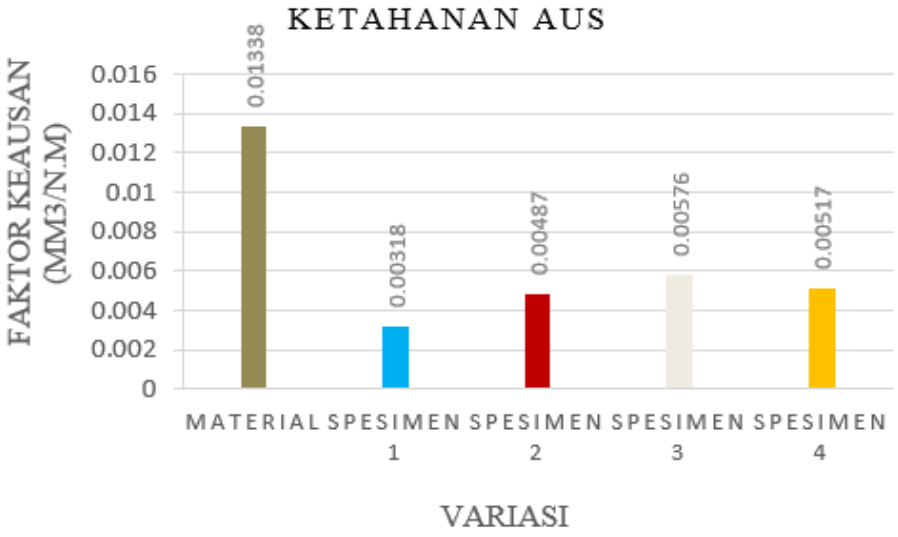



Figure 2: Wear Test Results

This phenomenon can be explained by the complex microstructural mechanisms in cobalt-based alloys. The wear resistance of Stellite alloys is determined not only by the volume fraction of hard carbides but also by the ability of the more ductile α-Co matrix to support these carbides and resist plastic deformation under shear stress from abrasive particles (Crook, 2022). In Specimen 4, the very high hardness is most likely due to the very high carbide density, which can cause matrix embrittlement. Under abrasive loading, this brittle matrix may not be able to effectively support the carbide particles, leading to the release of hard particles (carbide pull-out). These released particles then act as a third-party abrasive particle (third-body abrasive), which precisely speeds up the wear rate. In contrast, Specimen 1, although softer, possibly has its own optimal balance between hardness and toughness. Its matrix is more tenacious, capable of supporting the phase carbide in an effective way, absorbing part of the energy from the abrasion process, and preventing premature particle release. With that said, although its own violence is absolutely lower, microstructure Specimen 1 gives superior tribology performance in this test condition. It is necessary to note that without analysis of surface wear using

Scanning Electron Microscopy (SEM), the mechanism This proposed wear is of an inferential nature and requires more validation to carry on.

### 3.3 Microstructure Testing

#### 3.3.1 *Base Metal*

*The microstructure* of the ASTM A216 WCB *base metal can be seen in Figure 3.*

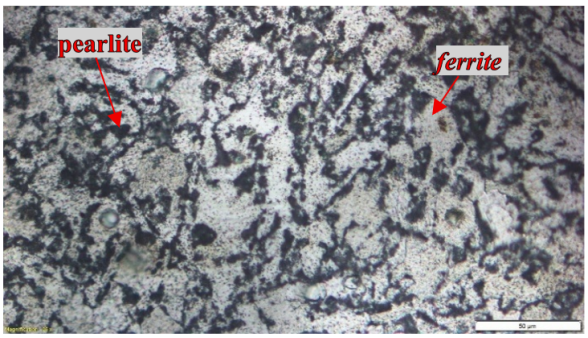



Figure: 3 *Microstructure of Base Metal*

Microstructural observations of the ASTM A216 WCB *base metal* show a typical medium carbon steel structure, consisting of ferrite (bright areas) and pearlite (dark, lamellar areas). This structure is consistent with the initial state of the material and does not show significant changes, indicating that this zone has not experienced high enough thermal cycling to trigger phase transformation.

#### 3.3.2 Buffer layer

The microstructure of the buffer layer looks like Figure 4.

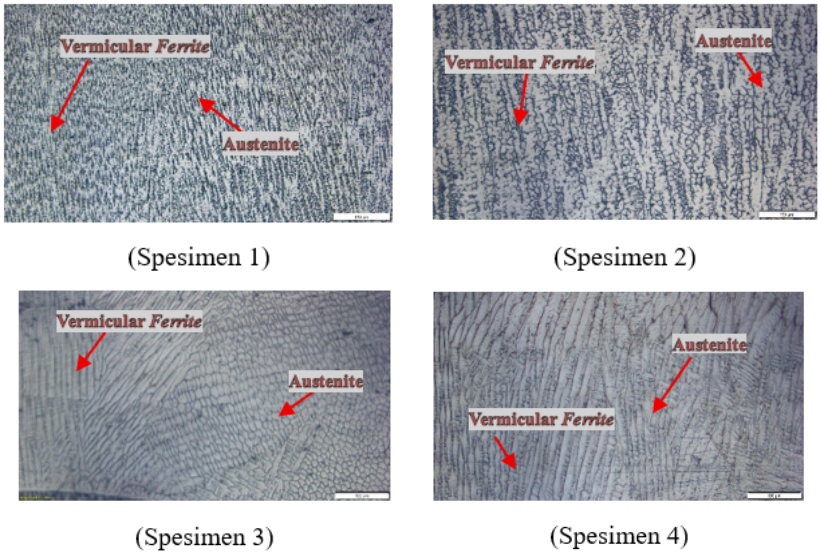



Figure 4: Microstructure Buffer layer

The microstructure of both types of buffer layers is dominated by a light austenite matrix with a vermicular ferrite phase (worm-shaped, dark) dispersed within it 4. The formation of this ferrite is important to prevent hot cracking during solidification. There are differences in morphology between specimens using ER308 and ER309. Specimens with the ER309 buffer layer (Specimens 3 and 4) tend to show a finer structure. This is due to the higher Cr and Ni contents in ER309, which produce a more stable austenite matrix and promote the formation of finer and more evenly distributed ferrite. This higher austenite stability provides better resistance to dilution and thermal stress, which are the main functions of the buffer layer (Kalyankar et al., 2020). An even distribution of ferrite tends to increase toughness while maintaining corrosion resistance (Hassel et al., 2025). Specimen 2 shows a more dominant and longer ferrite structure in the crystal orientation direction. This

increase in ferrite volume indicates a faster cooling rate or local composition differences due to variations in the welding process. Although ferrite can increase strength and heat resistance, excess ferrite can reduce corrosion resistance if it exceeds the optimum limit (Hassel et al., 2025). Specimen 3 shows a finer structure than 1 and 2. Ferrite is in the form of small and short ribbons, scattered among the austenite phase, which appears more dominant. This indicates that ER309, which has a higher Cr and Ni content, produces a more stable structure with austenite phase dominance. Meanwhile, in specimen 4, the ferrite structure appears to be more elongated, but not as much as in specimen 2. This structure indicates that although austenite is still dominant, there is an influence of the cooling rate and the addition of Cr elements in ER309, which triggers the formation of vermicular ferrite in larger quantities than in specimen 3.

### 3.3.3 Hardfacing Layer

The microstructure of the hardfacing layer is shown in Figure 5.

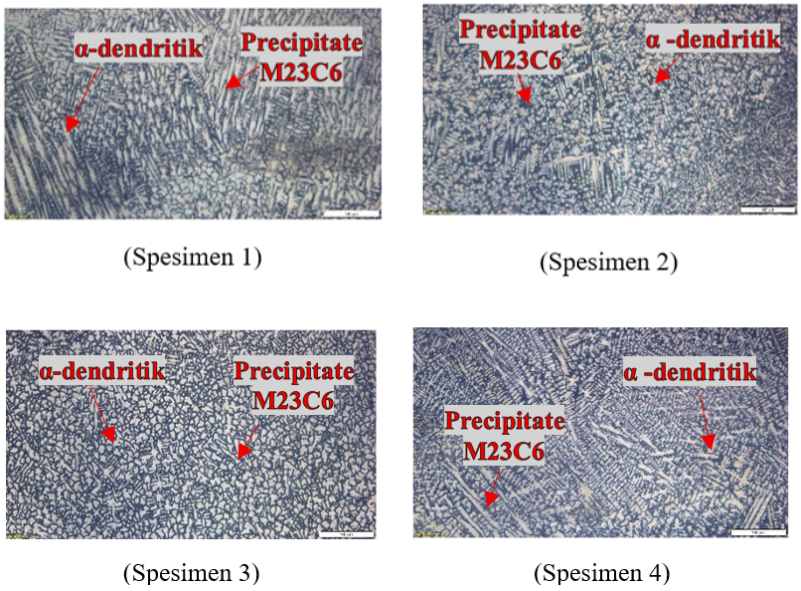



Figure 5: Microstructure of Hardfacing Layer

The microstructure of the Stellite 12 hardfacing layer (Figure 5) shows a classic hypoeutectic structure consisting of a dendritic cobalt-rich matrix (α-Co phase) with a eutectic network of hard precipitates in the interdendritic regions. Based on the known morphology and chemical composition of the Stellite 12 alloy, these precipitates are presumptively identified as complex carbides, most likely of the M23C6 and/or M7C3 type, where 'M' represents carbide-forming elements such as Cr, W, and Co. Definitive identification of these carbide phases requires advanced characterization techniques such as X-ray Diffraction (XRD) or Energy-Dispersive X-ray Spectroscopy (EDS) analysis in SEM, which is a limitation of this study but an important direction for future investigations. The number of hardfacing layers shows a clear influence on the microstructural fineness. The four-layer specimens (specimens 2 and 4) exhibit a finer dendritic structure and more evenly distributed carbide precipitates in the top layer than the two-layer specimens (specimens 1 and 3). This phenomenon occurs because the repeated thermal cycles of subsequent layer deposition act as in-situ heat treatments on the underlying layers, promoting grain refinement and structural homogenization. The finer and more homogeneous microstructure of Specimen 4 correlates well with its highest hardness value. Conversely, the slightly coarser structure of Specimen 1 likely provides higher matrix toughness, contributing to its superior wear performance.

## 4. CONCLUSION

This study systematically analyzes the effect of variations in buffer layer s (ER308 and ER309) and the number of Stellite 12 hardfacing layers (two and four layers) on ASTM A216 WCB material. Based on the results and discussion, several conclusions can be drawn, namely, increasing the number of hardfacing layers from two to four layers consistently increases the surface hardness. The highest hardness (477.89 HV) was achieved by specimens with ER309 buffer layer s and four layers of hardfacing. This increase is due to the reduced dilution effect of Fe from the substrate and the refinement of the microstructure due to repeated thermal cycles. A non-linear relationship between hardness and wear resistance was found. The highest abrasive wear resistance performance, characterized by the lowest wear rate (0.00318 $mm^3/N \cdot m$), was achieved by the specimen with an ER308 buffer layer and two layers of hardfacing, despite having a lower surface hardness (396.13 HV). The main contribution from this research is the demonstration of the empirical existence of the paradox of wear-hardness in this hardfacing system. This underlines that for application wear-out abrasives, optimization performance does not always mean maximizing violence, but rather reaching a balance of optimal microstructure between phase volume fraction and hard and tough carbide matrix for his supporters

## 5. ACKNOWLEDGMENT

The author team would like to express their gratitude to P3M Surabaya State Polytechnic of Shipbuilding for the support of the 2024 DIPA Research Grant Fund provided to the author team so that this research could be completed properly.

## 6. REFERENCES

Abdullah, MA, Razi, M., & Bahri, S. (2021). *The Effect of Tungsten Electrode Taper Angle on GTAW Weld Penetration*. *5* (1), 66–70.

Australian Stainless Steel Development Association. (2012). *Welding Dissimilar Metals. 316* (9), 2–4.

Azwinur, A., J., M., Y., & Zulkifli, Z. (2020). The Effect of Cooling Media on the Hardness and Toughness of Welding Results of AISI 1050 Material in the MAG Welding Process. *Jurnal POLIMESI, 18* (2), 124–130. Retrieved from http://e-jurnal.pnl.ac.id/index.php/polimesin/article/view/1924

Badheka, V. J., Basu, R., Omale, J., & Szpunar, J. (2016). Microstructural Aspects of the TIGG and A-TIG Welding Process of Dissimilar Steel Grades and Correlation to Mechanical Behavior. *Transactions of the Indian Institute of Metal, 6(9),* 1765–1773. doi: 10.1007/s12666-016-0836-5

Chotěborský, R., Hrabě, P., Müller, M., Savková, J., & Jirka, M. (2008). Abrasive wear of high chromium Fe-Cr-C hardfacing alloys. *Research in Agricultural Engineering, 54* (4), 192–198. doi: 10.17221/1/2008-rae

Crook, P. A. (2022). Guide to the Metallurgical, Corrosion, and Wear Characteristics of the Wrought Nickel and Cobalt Alloys. In Haynes International.

Darmo, S., & Prihadianto, BD (2023). The Effect of the Hard Facing Process on the Hardness and Microstructure of Bucket Teeth for Different Manganese Content. *Journal of Mechanical Engineering, 14* (3), 779–790. doi: 10.21776/jrm.v14i3.1084

Fauzi, YR, & Heka, AE (2024). The Effect of Heat Input on Dissimilar Combined GTAW-SMAW Welding of AISI 1045 Steel Material with SS 304 on Mechanical Properties. *Machine: Journal of Mechanical Engineering*, *10* (2), 47–52. doi: 10.33019/jm.v10i2.5406

Garbade, R.R., & Dhokey, N.B. (2021). Overview on Hardfacing Processes, Materials, and Applications. *IOP Conference Series: Materials Science and Engineering, 1017* (1). doi: 10.1088/1757-899X/1017/1/012033

Gonçalves Júnior, ER, de Oliveira, BF, Terrones, LAH, Simonassi, NT, & Monteiro, SN (2024). Effect of Welding Current on the Dilution and Mechanical Properties of Co–Cr Alloy Stellite-6 Coatings Applied to AISI 4130 Steel. *Coating*, *14* (12). doi: 10.3390/coatings14121591

Hassel, T.A., Kulbotten, I.M., Arbo, S.M., Rørvik, G., Brøtan, V., & Sørby, K. (2025). Corrosion, Impact Toughness, and Tensile Properties of Duplex Stainless Steels Manufactured by Directed Energy Deposition. *Metallurgical and Materials Transactions A: Physical Metallurgy and Materials Scienc*e, *56* (1), 269–293. doi: 10.1007/s11661-024-07586-3

Herizal, Hasrin, & Hanif. (2020). Analysis of the Effect of GTAW and SMAW Processes on the Toughness of Welding Joints of AISI 1050 Material welding is a process of joining two or more metal parts using heat energy and using additional materials or electrodes. *Journal of Welding Technology, 2* (1), 19–25. doi: http://dx.doi.org/10.30811/jowt.v2i1.1954

JC Casting. (2025). *How A216 WCB Powers Industrial Valve Applications.* JC Casting. Retrieved from https://www.jccasting.com/blog/a216-wcb-valve/

Jong, YE, Shin, GY, & Shim, D.S. (2021). Effect of P21 Buffer layer on Interfacial Bonding Characteristics of High-Carbon Tool Steel Hardfaced through Directed Energy Deposition. *Journal of Manufacturing Processes, 68,* 1596–1614. doi: 10.1016/j.jmapro.2021.07.002

Kalyankar, V., Naik, H., & Shah, S. (2020). Metallographic Characterization and Comparative Analysis of SS-309L and Inconel 625 as Buffer layer Materials on P91 Steel. *Practical Metallography, 57* (12), 828–852. doi: 10.3139/147.110667

Karadeniz, E., Ozsarac, U., & Yildiz, C. (2007). The Effect of Process Parameters on Penetration in Gas Metal Arc Welding Processes. *Materials and Design, 28* (2), 649–656. doi: 10.1016/j.matdes.2005.07.014

Luijan, J., Surin, P., & Eidhed, K. (2023). Investigation of ER308L and ER309L filler wires on dissimilar metals between carbon steel and 3CR12 ferritic stainless steel by GTAW through boiler fabrication in a sugar factory. *Materials Research Express, 10* (12). doi: 10.1088/2053-1591/ad0eaa

Maulana, R., Razi, M., & A Jalil, S. (2020). Stress Analysis on Plug Valve Using Simulation-Based Finite Element Method. *Journal of Applied Machine Science, 4* (2), 91. doi: 10.30811/jmst.v4i2.2013

Rana, T., Wu, J., Chung, G., Moeggenborg, K., & Gave, M. (2023). Study of Defects in 4H-SiC Epitaxy at Various Buffer layer Growth Conditions. *Defect and Diffusion Forum, 425,* 63–68. doi: 10.4028/p-72252k

Senthilkumar, S., Manivannan, S., Venkatesh, R., & Karthikeyan, M. (2023). Influence of Heat Input on the Mechanical Characteristics, Corrosion, and Microstructure of ASTM A36 Steel Welded by the GTAW Technique. *Heliyon, 9* (9). doi: 10.1016/j.heliyon.2023.e19708

Susetyo, FB, Sutrisno, HH, & Suryadewi, RA (2021). Study of Hardfacing Layer Results with Variations in Current and AWS A5.13 EFe2/A5.1 E7018 Electrodes. *Jurnal Asiimetri: Jurnal Ilmiah Rekayasa & Inovasi, 3,* 97–104. doi: 10.35814/asiimetri.v3i2.1944

Tandon, D., Li, H., Pan, Z., Yu, D., & Pang, W. (2023). A Review on Hardfacing, Process Variables, Challenges, and Future Works. *Metals, 13* (9). doi: 10.3390/met13091512

Yusim, AK, Fadila, MA, & Sarwoko, S. (2020). Valve Leak Testing Process on Km. Kendhaga Nusantara Using Hydrostatic Pressure Test. *Zona Laut Journal of Marine Science and Technology Innovation, 2* (3), 78–83. doi: 10.62012/zl.v1i3.11457